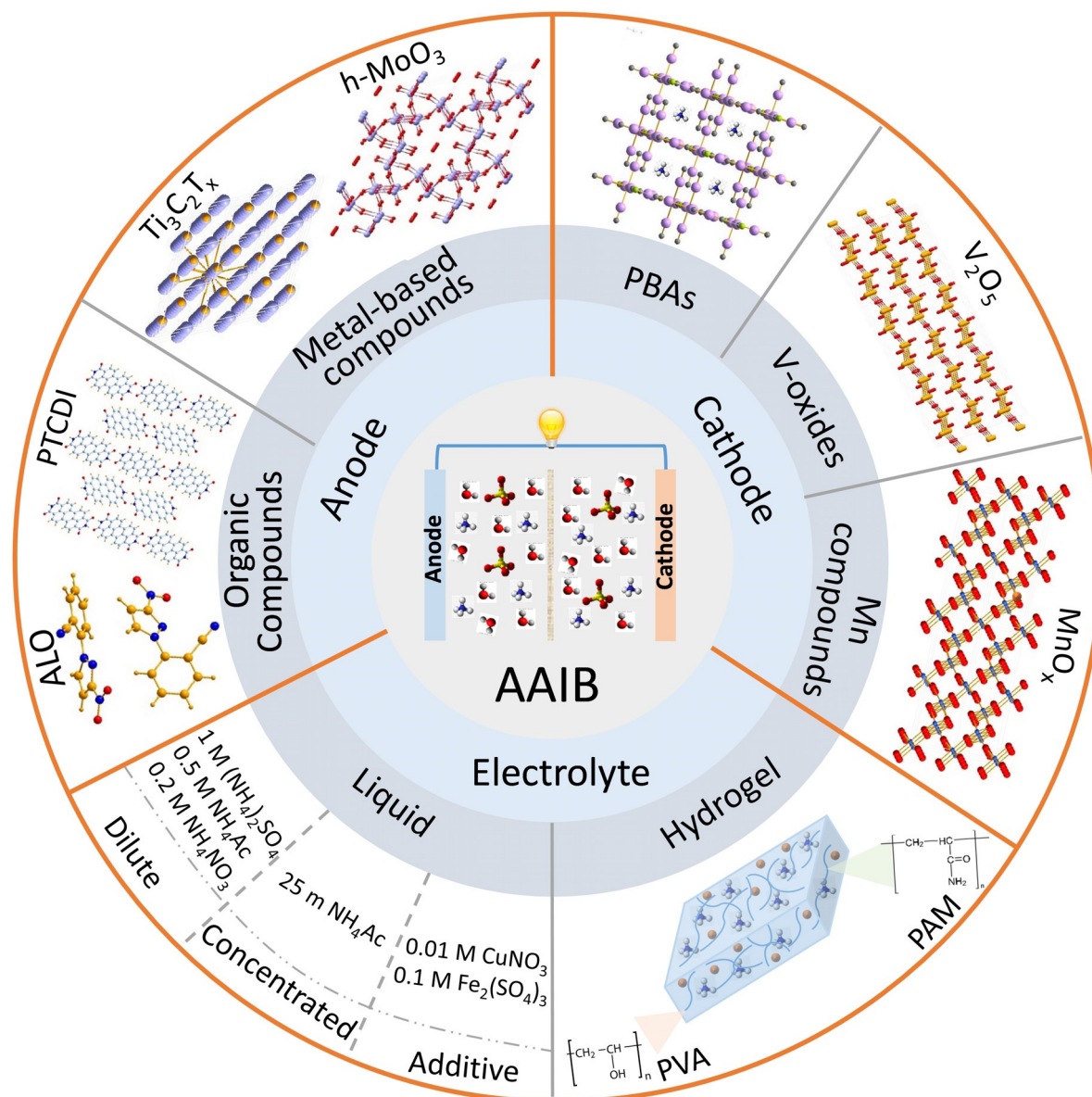


# The Emergence of Aqueous Ammonium-Ion Batteries

Jin Han, Alberto Varzi,\* and Stefano Passerini\*



**A**queous ammonium-ion ( $\text{NH}_4^+$ ) batteries (AAIB) are a recently emerging technology that utilize the abundant electrode resources and the fast diffusion kinetics of  $\text{NH}_4^+$  to deliver an excellent rate performance at a low cost. Although significant progress has been made on AAIBs, the technology is still limited by various challenges. In this Minireview, the most recent advances are comprehensively summarized and discussed, including cathode and anode materials as well as the electrolytes. Finally, a perspective on possible solutions for the current limitations of AAIBs is provided.

## 1. Introduction

The importance of exploiting renewable energy sources is evident in view of the increasingly extreme weather conditions caused by climate change.<sup>[1,2]</sup> To increase the use of renewable energy sources, effective and affordable energy storage systems (ESSs) are crucial, especially on large scales.<sup>[3]</sup> Despite the commercial success of lithium-ion batteries (LIBs) in the portable electronics and electromotive markets, safety issues arising from the flammable and volatile organic electrolytes impede their widespread application in large-scale stationary storage systems.<sup>[4]</sup> Moreover, the raw materials and manufacturing cost of LIBs also pose challenges.<sup>[5]</sup> To circumvent the aforementioned issues, extensive efforts have been made to develop alternative batteries that avoid the use of organic liquid electrolytes.<sup>[6]</sup>

Rechargeable rocking-chair LIBs with nonflammable aqueous electrolytes were first proposed by the Dahn group in 1994.<sup>[7]</sup> Aqueous batteries offer the advantages of inherent safety, low costs of the electrolyte and manufacturing, environmental benignity, high rate performance, and high tolerance to mishandling and misuse.<sup>[8]</sup> Additionally, aqueous rocking-chair batteries based on insertion-type electrodes offer improved round-trip efficiency compared to conventional aqueous systems, such as lead-acid batteries. After the first seminal paper was reported, aqueous rocking-chair batteries rapidly developed over the next two decades, but mostly at an academic level. In general, metallic cations, such as sodium ( $\text{Na}^+$ ),<sup>[9–11]</sup> potassium ( $\text{K}^+$ ),<sup>[12,13]</sup> zinc ( $\text{Zn}^{2+}$ ),<sup>[14–17]</sup> magnesium ( $\text{Mg}^{2+}$ ),<sup>[18,19]</sup> calcium ( $\text{Ca}^{2+}$ ),<sup>[20]</sup> and aluminum ( $\text{Al}^{3+}$ ),<sup>[21,22]</sup> are used as charge carriers. Recently, batteries based on the use of nonmetallic ammonium ( $\text{NH}_4^+$ ) ions as charge carriers have become appealing, as a result of the abundant resources for their synthesis, its relatively small hydrated ionic size (3.31 Å) that facilitates its fast diffusion in aqueous electrolytes, and low molar mass ( $18 \text{ g mol}^{-1}$ ; Figure 1 a).<sup>[23,24]</sup> In addition, aqueous solutions of  $\text{NH}_4^+$  are less corrosive and have lower potentials for the hydrogen evolution reaction (HER) compared to acidic electrolytes.<sup>[25,24]</sup> Moreover, ammonium salts are highly dissociated,<sup>[26]</sup> and thus provide improved ionic conductivity.<sup>[27]</sup> Interestingly,  $\text{NH}_4^+$  ions have a peculiar tetrahedral structure that differs from the spherical metal ions that have no preferred orientations.<sup>[28]</sup> The intercalation chemistry of  $\text{NH}_4^+$  ions in host electrode materials, therefore, differs from that of conventional metal-ion carriers.<sup>[29]</sup>

Pioneering work on AAIBs was first performed by the Cui group in 2012,<sup>[23]</sup> and, since then, multiple advancements have been made with regards to the electrode active materials and their  $\text{NH}_4^+$  storage mechanisms as well as to the electrolytes

(Figure 1 b). Developments at multiple levels have been reported, from half-cell to full-cell, from liquid electrolyte to hydrogel electrolyte, and from conventional cell setups to flexible cells. However, no review to date has examined this emerging field in detail. Thus, the advancements in electrode materials and electrolytes will be reviewed in the following sections. Additionally, the existing challenges as well as possible solutions are summarized to assist the further development of AAIBs.


## 2. Cathode Materials


Cathode materials play a crucial role in determining the capacity and cycling stability of full batteries.<sup>[30]</sup> Since the first report on AAIBs using Prussian blue analogues (PBAs) with an open framework as the  $\text{NH}_4^+$  host,<sup>[23]</sup> extensive efforts have been made to find alternative cathodes to further improve the capacity. So far, beyond PBAs, vanadium-based oxides and manganese-based compounds represent the two classes of materials with the most promising performance. Representative advances in  $\text{NH}_4^+$  cathode host materials are listed in Table 1 and the corresponding performances are summarized.

### 2.1. PBAs

PBAs possess the typical hexacyanometalate framework structure, which can be represented by the general formula  $\text{A}_x\text{PR}(\text{CN})_6$ .<sup>[41,42]</sup> In this formulation, P denotes the transition-metal cation coordinated with the nitrogen atom and  $\text{R}(\text{CN})_6$  represents the hexacyanometalate complexes which form a face-centered cubic open framework with large interstitial A sites (Figure 2 a).<sup>[43]</sup> Notably, the A sites can be partially or

[\*] J. Han, A. Varzi, S. Passerini  
Helmholtz Institute Ulm (HIU)  
Helmholtzstrasse 11, 89081 Ulm (Germany)  
and  
Karlsruhe Institute of Technology (KIT)  
P.O. Box 3640, 76021 Karlsruhe (Germany)  
E-mail: alberto.varzi@kit.edu  
stefano.passerini@kit.edu

 The ORCID identification number for one of the authors of this article can be found under: <https://doi.org/10.1002/anie.202115046>.

 © 2021 The Authors. Angewandte Chemie International Edition published by Wiley-VCH GmbH. This is an open access article under the terms of the Creative Commons Attribution Non-Commercial NoDerivs License, which permits use and distribution in any medium, provided the original work is properly cited, the use is non-commercial and no modifications or adaptations are made.

fully occupied by a number of different ions, and the ionic occupancy may change from 0 to 2.<sup>[44]</sup> According to previous reports, this kind of PBA with an open framework can deliver a high power capability and ultralong cycling.<sup>[45]</sup> Moreover, PBAs are economical materials that can be synthesized by easily scalable routes.<sup>[46]</sup>

The Cui group was the first to investigate the  $\text{NH}_4^+$  storage performance of copper hexacyanoferrate (CuHCF) and nickel hexacyanoferrate (NiHCF).<sup>[23]</sup> CuHCF demonstrated a single and sharp peak located at 1.02 V versus the standard hydrogen electrode (SHE) in 0.5 M  $(\text{NH}_4)_2\text{SO}_4$  electrolyte (Figure 2b). It is worth noting that the redox potential for the insertion/deinsertion of  $\text{NH}_4^+$  is higher than other metallic cations ( $\text{Li}^+$ ,  $\text{Na}^+$ , and  $\text{K}^+$ ). It was found that, as a consequence of their large ionic radii,  $\text{K}^+$  and  $\text{NH}_4^+$  are inserted into the PBA lattice in a completely dehydrated state. In contrast, the smaller  $\text{Li}^+$  and  $\text{Na}^+$  ions were partially hydrated during their insertion into PBA.<sup>[31,47]</sup> As demonstrated by La Mantia et al., larger ions are thermodynamically more favorable for intercalation compared with smaller ions. The necessity to remove the solvation shell upon intercalation explains the occurrence of the redox peak at different potentials for different ions.<sup>[48]</sup> The galvanostatic charge/discharge (GCD) profiles of CuHCF under different current densities (Figure 2c) also reveal an impressive high rate capability, even at  $2.5 \text{ A g}^{-1}$ .  $(\text{NH}_4)_{1.47}\text{Ni}[\text{Fe}(\text{CN})_6]_{0.88}$  (Ni-APW) has also been proposed as a cathode material by the Ji group. This material demonstrated a long cycle life and a high capacity retention of about 74% after 2000 cycles at  $2.5 \text{ A g}^{-1}$  with an average Coulombic efficiency (CE) of 99.4%.<sup>[24]</sup> During charge and discharge (Figure 2d), the typical (200) peak of Ni-APW gradually shifts from  $2\theta = 17.40^\circ$  to  $17.25^\circ$  upon  $\text{NH}_4^+$  insertion as a result of expansion of the unit cell, and then shifts back to the original position upon the release of  $\text{NH}_4^+$  (Figure 2e). More importantly, the first “rocking-chair” AAIB employing the Ni-APW cathode and a 3,4,9,10-



Jin Han received his M.S. in 2017 from Southwest University under the supervision of Prof. Maowen Xu and his PhD in 2021 from the Helmholtz-Institute Ulm (HIU) of the Karlsruhe Institute for Technology (KIT) under the supervision of Prof. Stefano Passerini. He is currently working as a post-doctoral fellow at HIU of KIT. His research interests are focused on the electrochemistry and electrolytes for aqueous batteries.



Alberto Varzi studied Chemistry of Materials at the University of Bologna (Italy) and received a PhD in 2013 from the Ulm University and the Center for Solar Energy and Hydrogen Research Baden-Württemberg (ZSW). After postdoctoral research at MEET battery research center—University of Muenster, in 2014 he joined the Helmholtz-Institute Ulm (HIU) of the Karlsruhe Institute for Technology (KIT). Since 2021 he has been Principal Investigator and leads the group “Electrochemistry of Materials and Interfaces”. His current research interests span from solid state to aqueous batteries, including beyond-Li systems.



Stefano Passerini is Professor at the Karlsruhe Institute of Technology, Helmholtz Institute Ulm. Formerly a Professor at the University of Muenster, he co-founded the MEET battery research center at the University of Muenster. His research activities are focused on electrochemical energy storage, with a special focus on improving the sustainability of high-energy batteries.

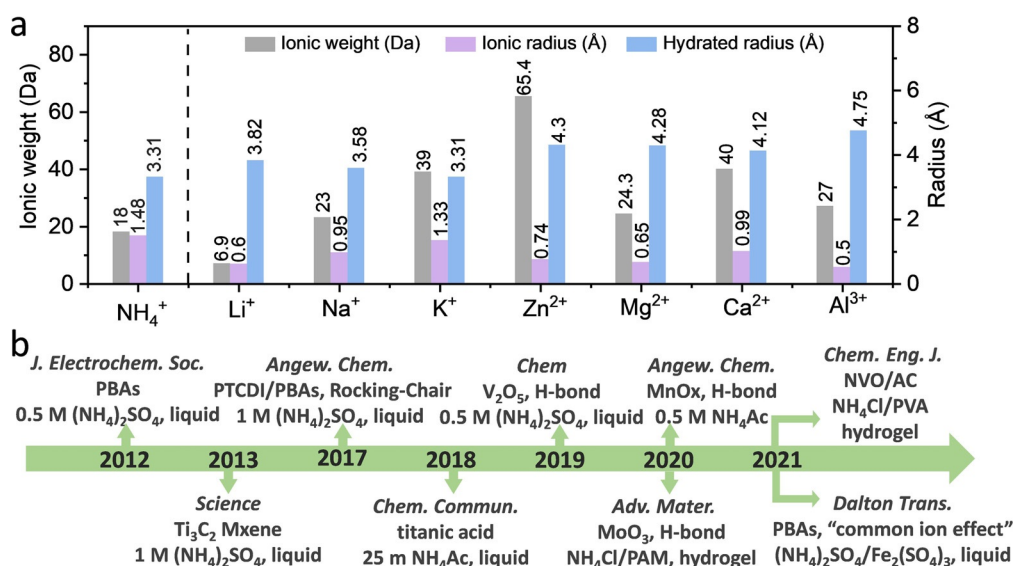


**Figure 1.** a) Comparison of the ionic weight, cation radius, and hydrated radius of the ammonium ion and conventional metal-ion charge carriers. Adapted and modified from Ref. [6] with permission from the American Association for the Advancement of Science. b) Timeline of the advancements in aqueous  $\text{NH}_4^+$  storage. Adapted and modified from Ref. [29] with permission from John Wiley and Sons.

**Table 1:** Performance of various  $\text{NH}_4^+$  cathode host materials.

Material	Working potential range	Electrolyte	Capacity [ $\text{mAh g}^{-1}$ ]	Current density [ $\text{A g}^{-1}$ ]	Capacity retention [%]	Cycling number	Ref.
<b>Cathode</b>							
CuHCF	0.6–1.4 V vs. SHE	0.5 M $(\text{NH}_4)_2\text{SO}_4$	55	0.5	91	500	[23]
NiHCF	0.4–1.0 V vs. SHE	0.5 M $(\text{NH}_4)_2\text{SO}_4$	38	0.5	91	500	[23]
Ni-APW	0.2–0.9 V vs. Ag/AgCl	1 M $(\text{NH}_4)_2\text{SO}_4$	51.3	0.3	74	2000	[24]
Berlin Green	–0.2–1.2 V vs. Ag/AgCl	0.5 M $(\text{NH}_4)_2\text{SO}_4$	80	5	88	50000	[31]
Bi-layered $\text{V}_2\text{O}_5$	–0.2–0.8 V vs. Ag/AgCl	0.5 M $(\text{NH}_4)_2\text{SO}_4$	70	5	80	30000	[32]
Na-FeHCFs	0–0.7 V vs. SCE	1 M $(\text{NH}_4)_2\text{SO}_4$	50	2	109.7	50000	[33]
CF@ $\text{NH}_4\text{V}_4\text{O}_{10}$	0.01–1.0 V vs. Ag/AgCl	1 M $(\text{NH}_4)_2\text{SO}_4$	103	0.1	82.5	100	[34]
N-CuHCF	0.5–1.0 V vs. SCE	0.01 M $\text{Cu}(\text{NO}_3)_2 + 2.0\text{ M } \text{NH}_4\text{NO}_3$	53.1	10	91.5	17000	[35]
CuHCF	0.3–1.1 V vs. SCE	2.0 M $\text{NH}_4\text{NO}_3$	72.5	5	72.5	30000	[36]
$\text{Fe}_4[\text{Fe}(\text{CN})_6]_3$	0.1–1.0 V vs. Ag/AgCl	1 M $(\text{NH}_4)_2\text{SO}_4$	40	1.8	88.9	2000	[37]
$\text{FeFe}(\text{CN})_6$	0.2–0.8 V vs. Ag/AgCl	0.1 M $\text{Fe}_2(\text{SO}_4)_3 + (\text{NH}_4)_2\text{SO}_4$	75	0.2	96.3	1000	[38]
MnOx	0–0.8 V vs. SCE	0.5 M $\text{NH}_4\text{Ac}$	87	5	94.7	10000	[29]
K-V-Fe PBAs	–0.1–1.2 V vs. SCE	1 M $(\text{NH}_4)_2\text{SO}_4$	93	2	91.44	2000	[39]
ferric vanadate	–0.4–1.25 V vs. Ag/AgCl	0.5 M $(\text{NH}_4)_2\text{SO}_4$	72.5	5	61	500	[40]

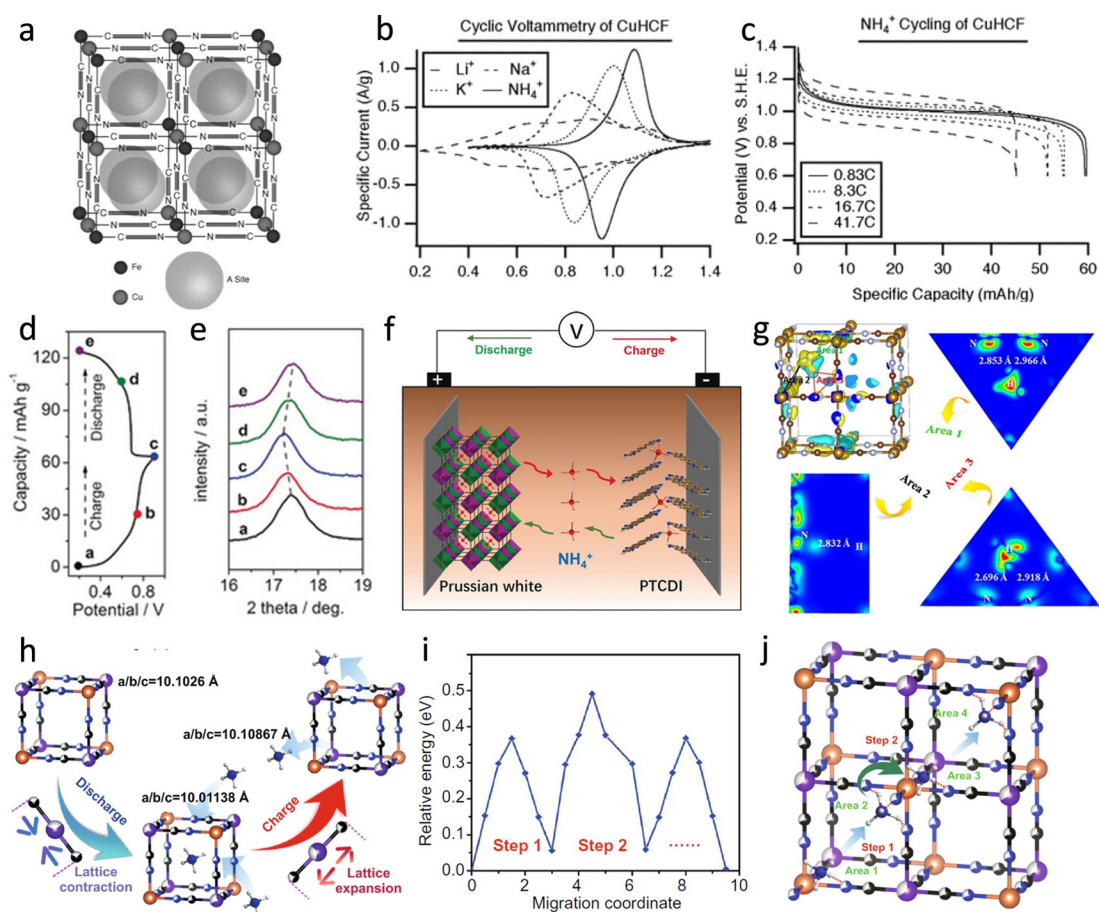


**Figure 2.** a) The unit cell of the PBA crystal structure with an open framework of octagonal hexacyanometalate groups. b) Cyclic voltammograms of CuHCF with inserted/deinserted  $\text{NH}_4^+$ ,  $\text{Li}^+$ ,  $\text{Na}^+$ , and  $\text{K}^+$  ions. c) GCD profiles of CuHCF hosting  $\text{NH}_4^+$  ions at various current densities. a–c) Reproduced from Ref. [23] with permission from the Electrochemical Society. d) Typical charge/discharge potential profiles of the Ni-APW electrode and e) the corresponding ex situ X-ray powder diffraction (XRD) patterns. f) Schematic representation of the rocking-chair AAIB reported by the Ji group. d–f) Reproduced from Ref. [24] with permission from John Wiley and Sons. g) The 3D electron density difference ( $\rho - \rho_{\text{corr}}$ ) and its 2D slices across Area 1, Area 2, and Area 3. Reproduced from Ref. [37] with permission from Elsevier. h) Schematic illustration of the evolution of the Fe–C bond distance and i) the changes in the diffusion activation energy during ammoniation/deammoniation processes. j) Schematic illustration of  $\text{NH}_4^+$  diffusion from the 48 g site to another. h–j) Reproduced from Ref. [36] with permission from Springer Nature.

perylene-tetracarboxylic diimide (PTCDI) anode (Figure 2f) displayed an average working voltage of about 1 V and an energy density of about  $43 \text{ Wh kg}^{-1}$  (based on the mass of both electrodes). In addition, the Berlin green framework demonstrated an excellent performance as an  $\text{NH}_4^+$  host, with an ultralong cycling performance of 50000 cycles with 78% capacity retention according to the reports of Ji and co-workers.<sup>[31]</sup> Such a Berlin green framework exhibited improved structural compatibility towards  $\text{NH}_4^+$  (de)insertion compared to  $\text{Na}^+$  and  $\text{K}^+$ . According to ex situ structural studies, this could be attributed to the nearly zero strain associated with the (de)insertion of  $\text{NH}_4^+$  in Berlin green. In fact, the hydration of the charge carrier plays a crucial role in the structural stability and, thus, the cycling performance of the host electrode materials. Electrochemical quartz crystal microbalance (EQCM) studies on PBA thin films<sup>[49–51]</sup> also confirmed that  $\text{Li}^+$  and  $\text{Na}^+$  are partially hydrated during their insertion into PBA, whereas  $\text{K}^+$  and  $\text{NH}_4^+$  are inserted into the lattice completely “naked”, although they diffuse in a hydrated form in the aqueous electrolyte bulk phase.<sup>[31,47]</sup>

$\text{NH}_4^+$ -rich copper hexacyanoferrate (N-CuHCF) was synthesized and investigated by the Shu group.<sup>[52]</sup> An outstanding capacity retention of 91.5% and 86.5% was reported over 17000 and 20000 cycles at 10 and  $18 \text{ A g}^{-1}$ , respectively. The reversible redox reaction based on  $\text{Fe}^{3+}/\text{Fe}^{2+}$  and  $\text{Cu}^{2+}/\text{Cu}^+$  couples in the N-CuHCF electrode was proven by X-ray photoelectron spectroscopy (XPS). To evaluate the effect of  $\text{NH}_4^+$  insertion on the stability of the host material, iron hexacyanoferrate ( $\text{Fe}_4[\text{Fe}(\text{CN})_6]_3$ ), density functional theory (DFT) calculations were performed by the Shu group.<sup>[37]</sup> The electron density difference diagrams (Figure 2g) show the formation of hydrogen bonds between the H atoms of  $\text{NH}_4^+$  and the N atoms of  $\text{Fe}_4[\text{Fe}(\text{CN})_6]_3$  to play a crucial role in the stabilization. In addition, the storage and diffusion mechanism of  $\text{NH}_4^+$  ions in copper hexacyanoferrate (CuHCF) were investigated by the same group, through the combination of theoretical and experimental methods.<sup>[36]</sup> Similarly, the formation of hydrogen bonds between the H atoms of  $\text{NH}_4^+$  and N atoms of CuHCF were revealed by ex situ solid-state nuclear magnetic resonance (SSNMR) and ex situ Fourier transform infrared (FTIR) spectroscopy. The in situ XRD patterns collected during the first cycle revealed the evolution of the highly reversible structure and led to the identification of a solid solution reaction mechanism. Figure 2h illustrates schematically the corresponding lattice contraction and expansion during the charge/discharge process. The activation energy for each diffusion step was also calculated (Figure 2i) and the diffusion process of the  $\text{NH}_4^+$  ions in CuHCF was

elucidated (Figure 2j). Once the  $\text{NH}_4^+$  ion is inserted into the 48 g site of CuHCF, a hydrogen bond is formed between the H atoms of the  $\text{NH}_4^+$  and N atoms in CuHCF. When the  $\text{NH}_4^+$  ion diffuses between two neighboring 48 g sites, a new hydrogen bond is formed. At the same time, energy is released during the diffusion, leading to a decrease in the total energy (Figure 2i). With the aim of improving the electrochemical activity and structural stability of the PBAs, novel K-V-Fe PBA nanocubes were synthesized by a one-step hydrothermal method. The material could deliver a high specific capacity of  $92.85 \text{ mAh g}^{-1}$  and a capacity retention of 91.44% after 2000 cycles at  $2 \text{ A g}^{-1}$ .<sup>[39]</sup> This strategy of doping PBAs with vanadium may be a feasible approach to obtain  $\text{NH}_4^+$  host electrode materials with improved performance.

## 2.2. V-Based Oxides

Although it has been established that hydrogen bonds influence the storage of  $\text{NH}_4^+$  ions in PBAs,<sup>[36]</sup> the role of hydrogen bonds in other materials remained elusive until the Ji group investigated the  $\text{NH}_4^+$  storage process in  $\text{V}_2\text{O}_5$ .<sup>[32]</sup> The bilayered  $\text{V}_2\text{O}_5$  electrode enabled  $\text{NH}_4^+$  insertion/deinsertion over 30000 cycles, and a strong hydrogen bond was observed between the  $\text{NH}_4^+$  ion and the oxygen atom of the  $\text{V}=\text{O}$  unit. As evidence, the FTIR spectra of the ammoniated  $\text{V}_2\text{O}_5$  was distinctly different from that of potassiated  $\text{V}_2\text{O}_5$ . Specifically, two bands appeared for the N-H vibrations in  $\text{NH}_4^+$  at around  $3050 \text{ cm}^{-1}$  and  $3150 \text{ cm}^{-1}$ , which are attributed to the N-H stretch with the H atom bonded with the VO host, and the N-H stretch of a nonbonded H atom, respectively.<sup>[32]</sup> The simulated structures of  $\text{V}_2\text{O}_5 \cdot 0.5\text{H}_2\text{O}$  (Figure 3a) without  $\text{NH}_4^+$  (left) and hosting  $\text{NH}_4^+$  (right) clearly reveal that  $\text{NH}_4^+$  ions play a role in cross-linking neighboring bilayers of  $\text{V}_2\text{O}_5$  by forming H bonds.<sup>[32]</sup> In addition, DFT calculations

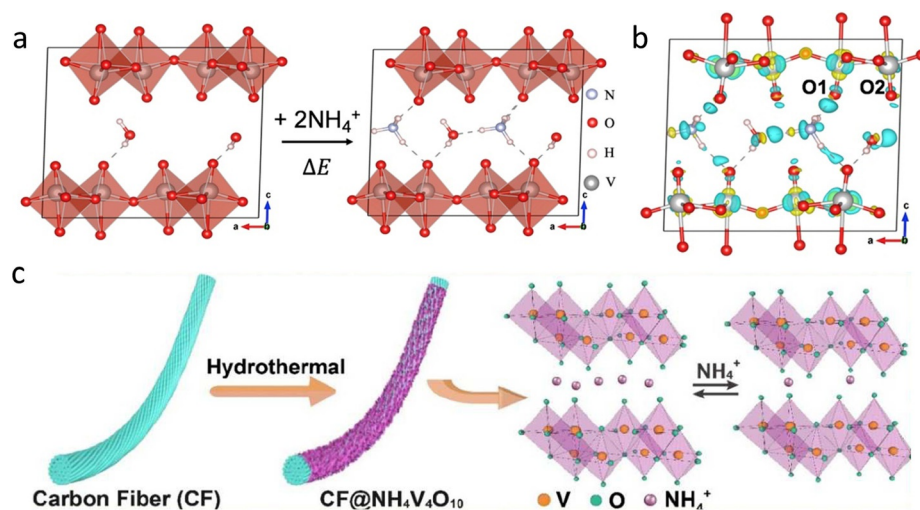


**Figure 3.** a) The computed electronic structure of  $\text{V}_2\text{O}_5 \cdot 0.5\text{H}_2\text{O}$  without  $\text{NH}_4^+$  (left) and hosting  $\text{NH}_4^+$  (right).  $\Delta E$  represents the host–ion interaction energy in this system. b) Plots of charge density difference for the ammoniated  $\text{V}_2\text{O}_5$  electrode, showing the movement of charge derived from the host–guest interaction. a,b) Reproduced from Ref. [32] with permission from Elsevier. c) Schematic illustration of the CF@ urchin-like  $\text{NH}_4\text{V}_4\text{O}_{10}$  and the evolution of the structure. Reproduced from Ref. [34] with permission from Elsevier.

provided further insights into the mechanism of ammonium storage. For the ammoniated  $V_2O_5$  electrode (Figure 3b), a small amount of charge is transferred from V through the O=V bond to an  $H\cdots O=V$  bond, thereby leading to the oxidation of V.<sup>[32]</sup>

Overall, despite their similar ionic sizes,  $NH_4^+$  and  $K^+$  display different electrochemical storage mechanisms in bilayer  $V_2O_5$ :  $NH_4^+$  forms H bonds with the oxygen atom in the V=O unit of bilayered  $V_2O_5$ , while  $K^+$  ions interact ionically with the host, thereby resulting in a lower the Gibbs free energy of the total ion–electrode system for hosting  $NH_4^+$  compared with  $K^+$ .<sup>[32]</sup> DFT calculations demonstrated that a total energy of  $-287.464$  eV is needed to form the final discharge product  $(NH_4)_{0.5}V_2O_5 \cdot 0.5H_2O$ , while  $-246.245$  eV is required to form  $K_{0.5}V_2O_5 \cdot 0.5H_2O$ . This explains once why the intercalation of  $NH_4^+$  in  $V_2O_5$  takes place at a higher potential than  $K^+$  ions.<sup>[32]</sup> As a consequence, a higher capacity can be delivered by the  $V_2O_5$  electrode at the same cut-off potential (vs. Ag/AgCl) during the storage of  $NH_4^+$  compared with the storage of  $K^+$  ions.<sup>[32]</sup> This interesting phenomenon was also identified for the 1,4,5,8-naphthalenetetracarboxylic dianhydride-derived polyimide (PNTCDA) electrode.<sup>[53]</sup> The easy formation and breaking of H bonds between  $NH_4^+$  and the  $V_2O_5$  layers is also responsible for the fast storage capability compared to other metallic charge carriers.

In terms of full-cell configurations, urchin-like  $NH_4V_4O_{10}$  coated on a carbon fiber was used as the cathode material and coupled with a polyaniline anode (Figure 3c).<sup>[34]</sup> The AAIB could deliver a high specific capacity of  $167$  mAh  $g^{-1}$  at a current density of  $0.1$  A  $g^{-1}$  and a proven high capacity retention over 1000 cycles. Similarly, layered iron vanadate (FVO) nanosheets were introduced as the  $NH_4^+$  host for the positive electrode, delivering a specific capacity of  $72.5$  mAh  $g^{-1}$  at  $5$  A  $g^{-1}$ .<sup>[40]</sup> In this case, the insertion of  $NH_4^+$  also involved the formation of a hydrogen bond between  $NH_4^+$  and the water structure in the FVO.<sup>[40]</sup>

### 2.3. Mn-Based Compounds

Mn-based oxides are established materials in the field of aqueous batteries,<sup>[55]</sup> especially as cathodes in Zn-ion batteries.<sup>[56–58]</sup> The Lu group was among the first to explore this class of materials for  $NH_4^+$  storage.<sup>[29]</sup> The electrodeposited manganese oxide ( $MnO_x$ ) demonstrated favorable  $NH_4^+$  storage in an ammonium acetate ( $NH_4Ac$ ) electrolyte. Specifically, the best performance was observed with a diluted  $0.5$  M  $NH_4Ac$  electrolyte, with a high specific capacity of  $176$  mAh  $g^{-1}$  at a current density of  $0.5$  A  $g^{-1}$  and a cycle life of over 10000 cycles. Moreover, a solid-solution behavior was observed for the  $NH_4^+$  insertion in the layered  $MnO_x$ . The results of the simulations (Figure 4a) suggest that the inserted  $NH_4^+$  ions not only form hydrogen bonds with the neighboring O atoms of  $MnO_2$ , but also with the adjacent lattice water

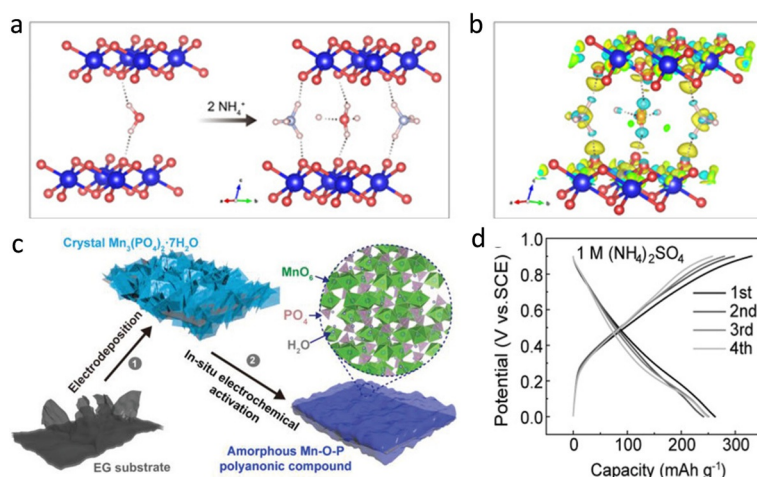


**Figure 4.** a) The lowest energy configuration of hydrous  $MnO_2$  hosting  $NH_4^+$  ions. b) Diagram of the charge density difference of the layered  $MnO_2$  structure after insertion of  $NH_4^+$  ions. a,b) Reproduced from Ref. [29] with permission from John Wiley and Sons. c) Schematic illustration of the fabrication process for amorphous manganese phosphate (AMP). d) GCD profiles of AMP in  $1$  M  $(NH_4)_2SO_4$  at a current density of  $1$  mA  $cm^{-2}$ . c,d) Reproduced from Ref. [54] with permission from John Wiley and Sons.

molecules. Charge transfer from  $NH_4^+$  to  $MnO_2$  layers through hydrogen bonds was demonstrated by the difference in the charge density (Figure 4b). Experimental and theoretical results indicated that the insertion/deinsertion of  $NH_4^+$  ions in  $MnO_x$  is associated with the formation/breaking of hydrogen bonds. From the calculated interaction energies, it was found that the insertion of  $NH_4^+$  ions into layered  $MnO_2$  is more energetically favorable than  $K^+$  ( $-4.12$  eV for  $NH_4^+$  and  $-3.22$  eV for  $K^+$ ).<sup>[29]</sup> Manganese phosphate is another type of potential Mn-based cathode for aqueous rechargeable devices (e.g. aqueous Na-ion batteries) in view of its high output potential and fast ion diffusion. The Liu group used an electrochemical method to prepare highly porous amorphous manganese phosphate (AMP) materials (Figure 4c)<sup>[54]</sup> that demonstrated reversible  $NH_4^+$  insertion/deinsertion (Figure 4d). This AMP electrode could also store other cations, namely,  $Na^+$ ,  $Zn^{2+}$ ,  $Mg^{2+}$ , and  $Ca^{2+}$  through a combined storage mechanism including both intercalation and conversion reactions.<sup>[54]</sup>

### 3. Anode Materials

Although several cathode materials, especially PBAs, have shown promising  $NH_4^+$  storage capability, full AAIBs are still in their infancy and exhibit unsatisfactory energy densities and durabilities. The anode materials, in particular, require further improvement. Therefore, several metal-based compounds and organic materials have been proposed. The most representative  $NH_4^+$  anode hosts are listed in Table 2 and their corresponding performances are summarized.

**Table 2:** Performance of various  $\text{NH}_4^+$  anode host materials.

Material	Working potential range	Electrolyte	Capacity [ $\text{mAh g}^{-1}$ ]	Current density [ $\text{A g}^{-1}$ ]	Capacity retention [%]	Cycling number	Ref.
<b>Anode</b>							
PTCDI	−1.05–0.2 V vs. Ag/AgCl	1 M $(\text{NH}_4)_2\text{SO}_4$	105	1.2	89.5	500	[24]
titanic acid	−1.3–−0.6 V vs. Ag/AgCl	25 M $\text{NH}_4\text{Ac}$	70	5	80	125	[59]
CF@PANI	−0.1–0.5 V vs. Ag/AgCl	1 M $(\text{NH}_4)_2\text{SO}_4$	77	0.1	81.8	100	[34]
h-MoO <sub>3</sub>	−0.5–0.8 V vs. SCE	$\text{NH}_4\text{Cl}$ /PAM, hydrogel	35	18	94	100000	[60]
PNTCDA	−1–0 V vs. Ag/AgCl	25 M $\text{NH}_4\text{Ac}$	106	8	88.7	30000	[53]
PI/NDC/ CNT	−0.9–0.1 V vs. SCE	1 M $(\text{NH}_4)_2\text{SO}_4$	164	0.5	87.9	5000	[61]
ALO	−0.7–0 V vs. Ag/AgCl	1 M $(\text{NH}_4)_2\text{SO}_4$	120	10	80	1500	[62]

### 3.1. Metal-Based Compounds

A large family of 2D materials called “MXenes”, which possess both considerable electrical conductivity as well as hydrophilic surfaces, have been extensively investigated by many groups, in particular the Gogotsi group.<sup>[63,64]</sup> As host materials for  $\text{Li}^+$  ions in non-aqueous electrolyte, MXenes can provide reversible electrochemical lithiation/delithiation, as shown by in situ XRD studies. The expanded *c*-parameter confirms that the  $\text{Li}^+$  ions are inserted between the  $\text{Ti}_2\text{C}$  layers.<sup>[65,66]</sup> The electrochemical intercalation of other cations, including  $\text{NH}_4^+$ , into  $\text{Ti}_3\text{C}_2\text{T}_x$  in aqueous solution was first reported in 2013.<sup>[67]</sup>

In addition, other Ti-based materials relying on the  $\text{Ti}^{4+}/\text{Ti}^{3+}$  redox couple have been widely employed as the anode materials of aqueous batteries (e.g. aqueous Li-ion and Na-ion batteries).<sup>[68–70]</sup> For example, amorphous “titanic acids”, denoted as  $\text{TiO}_x(\text{OH})_{4-2x}$ , were reported as anode hosts for  $\text{NH}_4^+$  ions.<sup>[59]</sup> It was found that a strong  $\text{NH}_4^+$ -O-Ti hydrogen bond between the inserted  $\text{NH}_4^+$  ion and the titanic acid is formed, as verified by ex situ FTIR spectroscopy. Specifically, the broad band corresponding to the Ti–O bond in the 1550–1600  $\text{cm}^{-1}$  range of the ammoniated titanic acid electrode spectrum experiences a clear red-shift compared with the pristine sample.

Orthorhombic molybdenum oxide ( $\alpha$ -MoO<sub>3</sub>) demonstrated a good performance with regards to Li-ion storage.<sup>[71]</sup> Interestingly, hexagonal MoO<sub>3</sub> (h-MoO<sub>3</sub>), which has of a tunnel structure, provides a larger hosting spatial location compared with  $\alpha$ -MoO<sub>3</sub>, thus enabling increased superionic conductivity (ca. 550 times) compared to  $\alpha$ -MoO<sub>3</sub>.<sup>[72]</sup> As a result, the Zhi group studied h-MoO<sub>3</sub> as an  $\text{NH}_4^+$  host material, which delivered a reversible capacity of 32  $\text{mAh g}^{-1}$  at 15  $\text{A g}^{-1}$  and 94% capacity retention over 100000 cycles.<sup>[60]</sup> Such a performance could be attributed to the fast diffusion pathway and ultrafast kinetics of  $\text{NH}_4^+$  ions in h-MoO<sub>3</sub>. GCD

profiles (Figure 5a) and XRD results at selected states of charge (Figure 5b) showed that the (320), (410), and (404) diffraction peaks shifted slightly to lower angles during the discharge process as a result of  $\text{NH}_4^+$  insertion, while they reversibly shifted back to the initial position during deinsertion.<sup>[60]</sup> The mechanism of  $\text{NH}_4^+$  insertion in h-MoO<sub>3</sub> was also investigated by SSNMR (Figure 5c). It was noted that the signal position corresponding to crystalline H<sub>2</sub>O remained unchanged, whereas the signals at 5.3 ppm and 5.8 ppm experienced reversible transitions during the  $\text{NH}_4^+$  insertion/deinsertion process, as a result of the changing chemical environment of the hydrogen bonds formed between the  $\text{NH}_4^+$  ions and different structural oxygen atoms in h-MoO<sub>3</sub>.<sup>[60]</sup> The formation/breaking of hydrogen bonds plays a critical role during the reversible insertion/deinsertion of  $\text{NH}_4^+$  in h-MoO<sub>3</sub>, and guarantees ultrafast kinetics and outstanding durability during cycling.<sup>[60]</sup> Modeling studies were performed on three individual states (a, b, c), in which the hydrogen bond numbers are 3, 4, and 2, respectively (Figure 5d–f). The results agreed well with the SSNMR data.<sup>[60]</sup> In short, the building/breaking of hydrogen bonds originating from the interaction between H atoms of  $\text{NH}_4^+$

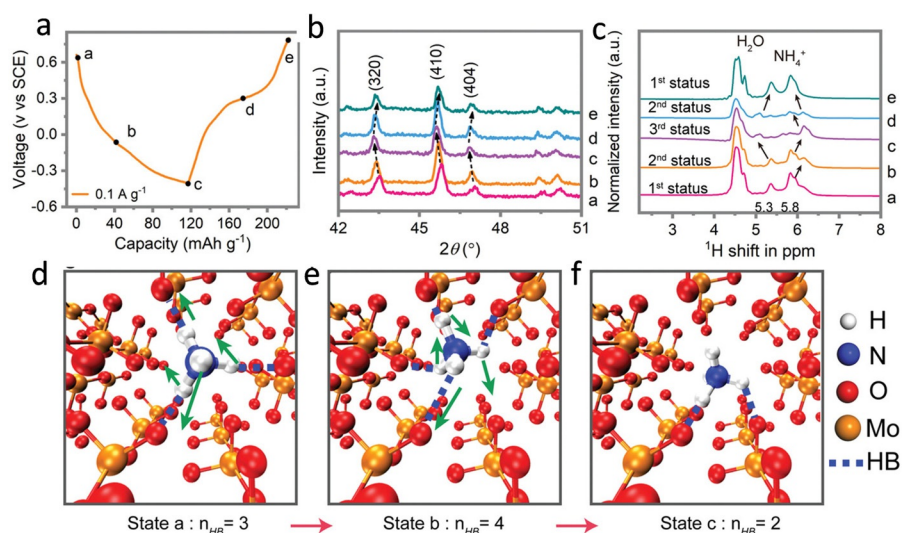


**Figure 5.** a) GCD profiles of the selected states. b) XRD results and c) solid-state  $^1\text{H}$  MAS NMR spectra corresponding to different charge/discharge states in (a). d–f) Evolution of the interaction between h-MoO<sub>3</sub> and  $\text{NH}_4^+$  in three stages during the  $\text{NH}_4^+$  diffusion process. a–f) Reproduced from Ref. [60] with permission from John Wiley and Sons.

and the adjoining O atoms in h-MoO<sub>3</sub> is responsible for the excellent electrochemical properties.<sup>[60]</sup>

### 3.2. Organic Compounds

Organic compounds have become of great interest as battery materials because of their low cost, eco-friendliness, and capability of accepting ions of different sizes.<sup>[74,75]</sup> Organic electrode materials mainly consist of n-type and p-type compounds.<sup>[76,77]</sup> In n-type compounds, the negatively charged N<sup>-</sup> sites would be neutralized to the neutral state (N) by the interacting cations (i.e. Li<sup>+</sup>, Na<sup>+</sup> or K<sup>+</sup>), whereas in p-type compounds, the positively charged P<sup>+</sup> sites would be neutralized to the neutral state (P) by the interacting anions (i.e. TFSI<sup>-</sup>, ClO<sub>4</sub><sup>-</sup> or PF<sub>6</sub><sup>-</sup>).<sup>[78]</sup>

3,4,9,10-Perylenetetracarboxylic diimide (PTCDI) was reported as an anode material by the Ji group.<sup>[24]</sup> In the first cycle, the insertion/deinsertion capacity values were 127.9 and 158.9 mAh g<sup>-1</sup>, respectively, at a current density of 0.24 A g<sup>-1</sup> (Figure 6a). After stabilization, the charge capacity at the 10th cycle was about 119 mAh g<sup>-1</sup> with an increased Coulombic efficiency (CE) of about 95%. The two reversible charge/discharge plateaus can be attributed to the reversible electrochemical enolization reaction of carbonyl groups in the PTCDI structure.<sup>[79]</sup> Clearly, the CE still needs to be improved to satisfy the requirements for practical application. The proposed mechanism for the insertion of NH<sub>4</sub><sup>+</sup> ions in the PTCDI anode is depicted in Figure 6b. Specifically, the C=O bonds located at diagonal positions in the PTCDI structure would be broken and O-NH<sub>4</sub><sup>+</sup> would be formed.<sup>[24]</sup> In total, two NH<sub>4</sub><sup>+</sup> ions could be accommodated per PTCDI molecule. Polyimide (PI) also attracted attention as an ammonium-ion host. Five types of PIs based on different dianhydrides and diamine monomers were successfully synthesized by Zhan

et al. All the PIs demonstrated a high CE of about 100% during the electrochemical measurements.<sup>[80]</sup> PI was also investigated by the Zhang group as an anode host in 1M (NH<sub>4</sub>)<sub>2</sub>SO<sub>4</sub> aqueous electrolyte and the NH<sub>4</sub><sup>+</sup> storage mechanism was demonstrated to be similar to that of PTCDI (Figure 6c).<sup>[73]</sup> As a result, PI could deliver a high specific capacity of 157.3 mAh g<sup>-1</sup> at 0.5 A g<sup>-1</sup>, and 107.7 mAh g<sup>-1</sup> at 10 A g<sup>-1</sup> (Figure 6e). The individual cyclic voltammograms (CVs) of a PI anode and the poly(2,2,6,6-tetramethylpiperidinyloxy-4-yl methacrylate) (PTMA; Figure 6d) demonstrate their suitability for use in ammonium dual-ion batteries (ADIBs). Furthermore, a flexible, electroactive, composite nanofiber electrode consisting of PI, N-doped carbon, and carbon nanotubes (PI/NDC/CNTs) with a highly interconnected conductive porous structure was prepared by electrospinning and a subsequent in situ pyrolysis/imidization treatment. The material delivered a reversible capacity of 161 mAh g<sup>-1</sup> at 0.5 A g<sup>-1</sup> and a capacity retention of over 87.9% after 5000 cycles.<sup>[61]</sup> Moreover, the ADIBs with the PI/NDC/CNT anode and PANI cathode could achieve a specific energy density of 114.3 Wh kg<sup>-1</sup> at a power density of 18.6 kW kg<sup>-1</sup> (based on the cathode active material mass). Alloxazine (ALO) is also a promising organic anode material that possesses a high theoretical specific capacity (250 mAh g<sup>-1</sup>), low redox potential, remarkable cycling stability, and considerable rate performance.<sup>[62]</sup> The CV curves of the ALO anode demonstrated a reduction potential at around -0.6 V vs. Ag/AgCl (Figure 6f). The combination of the ALO anode and a Ni-APW cathode with an average operation potential of +0.6 V vs. Ag/AgCl, resulted in a full cell with 1.2 V. Almost no voltage decay nor polarization increase was observed upon galvanostatic cycling at an increasing C-rate (Figure 6g).

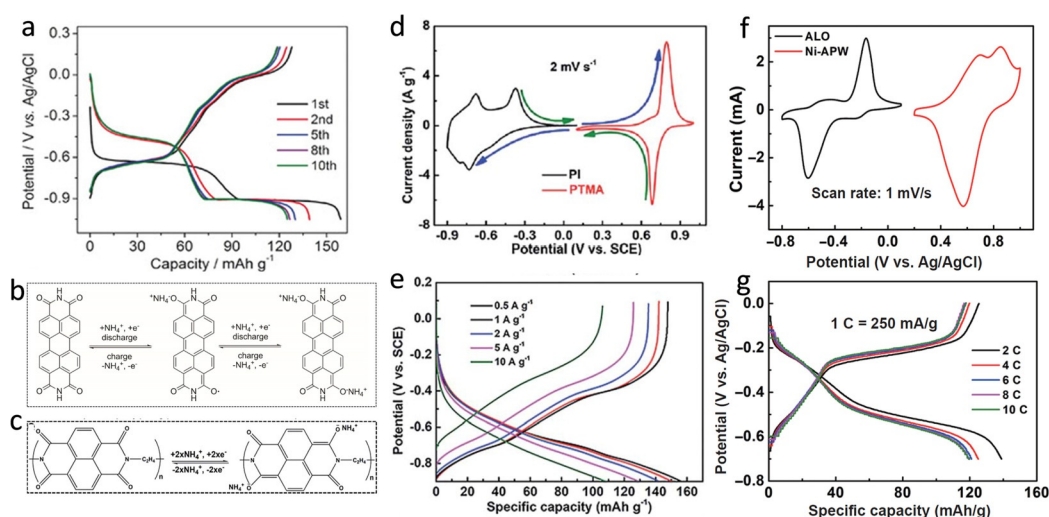


**Figure 6.** a) GCD profiles curves of a PTCDI anode at a current density of 0.24 A g<sup>-1</sup>. b) Proposed mechanism of NH<sub>4</sub><sup>+</sup> insertion in the PTCDI anode. a,b) Reproduced from Ref. [24] with permission from John Wiley and Sons. c) Proposed mechanism of NH<sub>4</sub><sup>+</sup> insertion in the PI anode. d) Comparison of the CV curves of the PI anode and PTMA cathode. e) GCD profiles of the PI anode at various current densities. c–e) Reproduced from Ref. [73] with permission from The Royal Society of Chemistry. f) GCD profiles of the alloxazine (ALO) anode at various current densities. g) Cyclic voltammograms of the ALO anode and Ni-APW cathode at 1 mV s<sup>-1</sup>. f,g) Reproduced from Ref. [62] with permission from Springer Nature.



## 4. Electrolytes

In addition to the active electrode materials, extensive efforts have been made in the development of suitable aqueous electrolytes. The two main classes of electrolyte are conventional liquids and hydrogels.

### 4.1. Aqueous Liquid Electrolytes

The aqueous 0.5 M  $(\text{NH}_4)_2\text{SO}_4$  liquid electrolyte was the first electrolyte employed in combination with the PBA cathode. In this case, the pH value of the electrolyte was adjusted to 2 by the addition of sulfuric acid with the aim of shifting the electrochemical stability window (ESW) to the anodic side.<sup>[23]</sup> Since then, an aqueous 1 M  $(\text{NH}_4)_2\text{SO}_4$  liquid electrolyte was also employed in combination with  $\text{Ti}_3\text{C}_2$  Mxene,<sup>[67]</sup> PBAs, and PTCDI electrode materials.<sup>[24]</sup> Interestingly, the aqueous 1 M  $(\text{NH}_4)_2\text{SO}_4$  electrolyte was also selected for a flexible AAIB full cell consisting of a  $\text{CF@NH}_4\text{V}_4\text{O}_{10}$  cathode and a  $\text{CF@PANI}$  anode (Figure 8a).<sup>[34]</sup>

Other types of salts, such as  $\text{NH}_4\text{Cl}$ ,<sup>[60]</sup>  $\text{NH}_4\text{Ac}$ ,<sup>[29,53]</sup> and  $\text{NH}_4\text{NO}_3$ ,<sup>[36]</sup> have also been studied for AAIB electrolytes. It should be noted that the anion can affect the acid–base properties of the electrolyte and, therefore, the stability window. For example, the 0.5 M  $\text{NH}_4\text{Ac}$  electrolyte has an almost neutral pH value (ca. 6.8), whereas 1 M  $(\text{NH}_4)_2\text{SO}_4$  is slightly more acidic (ca. pH 6.0). Additionally, the anion would also have a distinct influence on the solvation structure of the cation, as well as lead to an anion-derived solid electrolyte interphase (this aspect has yet to be investigated). Besides changing the type of salt, the properties of the electrolyte can be further modified by controlling the salt

concentration or by adding additives to enhance the performance of the AAIB.<sup>[35,38,53]</sup>

Highly concentrated electrolytes or water-in-salt electrolytes (WiSEs) have attracted much attention on account of their merits, such as enabling a wide ESW, inhibiting parasitic side reactions, and suppressing active material dissolution.<sup>[81]</sup> For example, the Ji group reported a WiSE composed of 25 M  $\text{NH}_4\text{Ac}$  which showed a ESW that was broadened to 2.95 V in 25 M  $\text{NH}_4\text{Ac}$  compared to 2.25 V in 1 M  $\text{NH}_4\text{Ac}$  (Figure 7a). Although the titanate acid electrode displayed superior electrochemical performance in 25 M  $\text{NH}_4\text{Ac}$  than in 1 M  $\text{NH}_4\text{Ac}$ ,<sup>[59]</sup> the electrochemical performance can still be improved. Thus, a PNTCDA electrode was studied with the 25 M  $\text{NH}_4\text{Ac}$  electrolyte by the same group.<sup>[53]</sup> Notably, a PNTCDA electrode delivered an improved capacity of about  $160 \text{ mAh g}^{-1}$  with an initial Coulombic efficiency (ICE) of 88.9% in the 25 M  $\text{NH}_4\text{Ac}$  electrolyte, whereas inferior reversibility and a clear capacity fading could be observed in 1 M  $\text{NH}_4\text{Ac}$  (Figure 7b,c). Upon continuous cycling, the CE improved from 93.0 to about 99.4% in the WiSE. Interestingly, the opposite trend was observed for an  $\text{MnO}_x$  electrode in an  $\text{NH}_4\text{Ac}$  electrolyte (Figure 7d–f).<sup>[29]</sup> The  $\text{MnO}_x$  electrode exhibited a more stable cycling performance in 0.5 M  $\text{NH}_4\text{Ac}$  than in 8 M  $\text{NH}_4\text{Ac}$ . The concentrated  $\text{NH}_4\text{Ac}$  electrolyte would negatively affect the capacity retention of  $\text{MnO}_x$ , due to the structural degradation caused by excessive storage of  $\text{NH}_4^+$  ions in the oxide lattice.<sup>[29]</sup>

The Shu group has proven that the addition of functional additives to the electrolyte is a successful strategy. Specifically, 0.1 M  $\text{Fe}_2(\text{SO}_4)_3$  was added to the  $\text{NH}_4(\text{SO}_4)_2$  electrolyte, which enabled the FeHCF cathode to operate with a high capacity retention of 96.3% after 1000 cycles.<sup>[38]</sup> The improved performance was attributed to the so-called “common

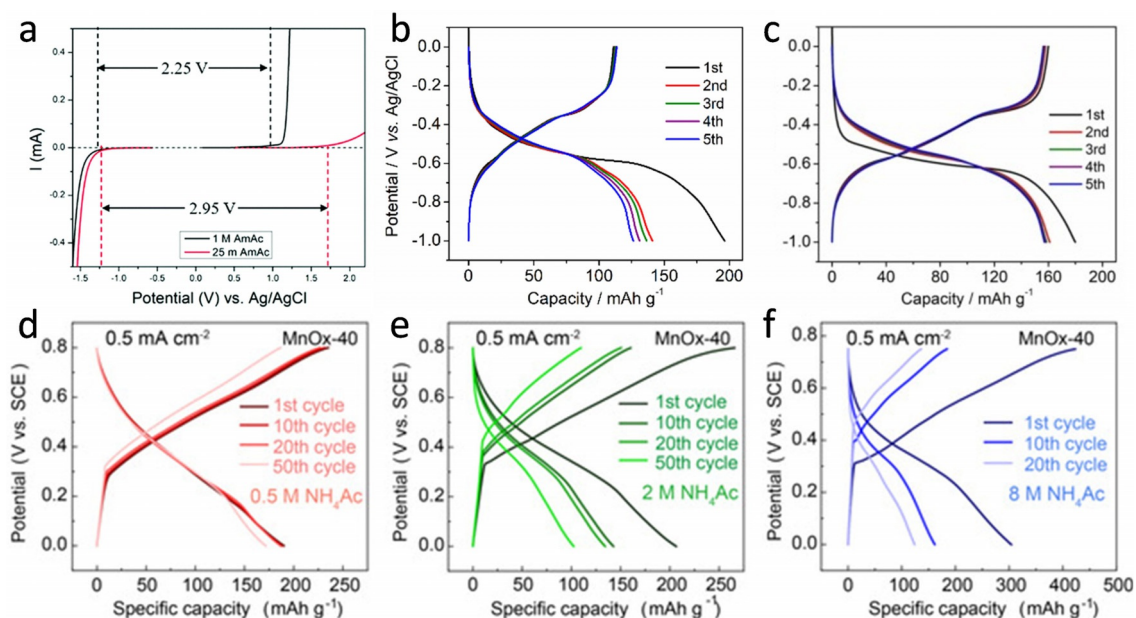


**Figure 7.** a) Linear sweep voltammograms recorded at  $1 \text{ mVs}^{-1}$  in 1 M and 25 M ammonium acetate ( $\text{NH}_4\text{Ac}$ ) electrolytes. Reproduced from Ref. [59] with permission from The Royal Society of Chemistry. GCD profiles of PNTCDA in b) 1 M  $\text{NH}_4\text{Ac}$  and c) 25 M  $\text{NH}_4\text{Ac}$  at  $0.16 \text{ Ag}^{-1}$ . Reproduced from Ref. [53] with permission from Elsevier.<sup>[53]</sup> GCD profiles of electrodeposited  $\text{MnO}_x$  in d) 0.5 M, e) 2 M, and f) 8 M  $\text{NH}_4\text{Ac}$  electrolyte. d–f) Reproduced from Ref. [29] with permission from John Wiley and Sons.

ion effect".<sup>[82,83]</sup> Similarly, a small concentration (0.01M) of  $\text{Cu}(\text{NO}_3)_2$  was also added to a  $\text{NH}_4\text{NO}_3$  aqueous electrolyte.<sup>[35]</sup> In combination with a  $\text{CuHCF}$  cathode, this helped avoid dissolution of  $\text{Cu}^{2+}$  ions from the active material, thus preserving its integrity.

It is worth mentioning that protons can compete with ammonium ions for intercalation in both anode and cathode materials. The Ji group found that PBAs can accommodate protons in a 2M  $\text{H}_2\text{SO}_4$  electrolyte by a diffusion-free Grotthuss mechanism.<sup>[84]</sup>  $\text{MnO}_2$  can also host protons in the mildly acidic electrolytes used for Zn-based batteries.<sup>[85,86]</sup> Of course, the contribution of proton intercalation is highly dependent on the acidity and concentration of the electrolyte. For example, in neutral/near-neutral  $\text{NH}_4\text{Ac}$  electrolytes, ammonium-ion intercalation was found to be the dominating mechanism in  $\text{MnO}_2$  cathodes (Figure 7 e,f).<sup>[29]</sup> The effect of proton/hydronium insertion was also studied by comparing the electrochemical behavior of a  $\text{V}_2\text{O}_5$  electrode in highly diluted  $\text{H}_2\text{SO}_4$  and 0.5M  $(\text{NH}_4)_2\text{SO}_4$  solution having a similar pH value of 5.3. Compared to ammonium-ion storage, the contribution from proton intercalation was found to be negligible.<sup>[32]</sup>

#### 4.2. Hydrogel Electrolytes

Hydrogels are composed of a cross-linked network of polymer chains with interstitial spaces filled with water.<sup>[8889]</sup> A large amount of water can be trapped in the framework on account of the charged functional groups on the polymer chain.<sup>[90]</sup> Thus, the water activity is effectively suppressed by the extensive interaction between the water and polymer chains.<sup>[91]</sup> Consequently, hydrogel electrolytes for AAIBs are gradually gaining attention. Pioneering work on this topic has been done by the Zhi group, who reported a polymeric hydrogel electrolyte constituted of polyacrylamide (PAM) and  $\text{NH}_4\text{Cl}$ .<sup>[60]</sup> A flexible quasi-solid-state full AAIB with a sandwich structure was further assembled by pairing it with a  $\text{CuFe}$  PBA cathode and  $\text{h-MoO}_3$  anode (Figure 8b). It is worth noting that a mechanical strength of 5.84 MPa and an ionic conductivity of  $8.7 \times 10^{-3} \text{ Scm}^{-1}$  could be obtained with this PAM electrolyte, which may be ideal for a flexible device needing a good mechanical and electrochemical performance. The cell delivered an outstanding capacity retention of 90.3% after 600 cycles at  $1 \text{ Ag}^{-1}$ . Similarly, a  $\text{NH}_4\text{Cl}$ /polyvinyl alcohol (PVA) hydrogel electrolyte allowed improved  $\text{NH}_4^+$  storage performance of ammonium vanadium oxide (NVO) by suppressing the dissolution of NVO.<sup>[87]</sup> Furthermore, a flexible quasi-solid-state device consisting of an  $\text{NVO@CFF}$  cathode,  $\text{AC@CFF}$  anode, and the hydrogel electrolyte was assembled (Figure 8c). In short, hydrogel electrolytes are an exciting class of electrolytes for developing leakless and flexible devices.

### 5. Summary and Perspectives

As a consequence of the fast diffusion and the unique storage mechanism of  $\text{NH}_4^+$  ions in aqueous solution, AAIBs

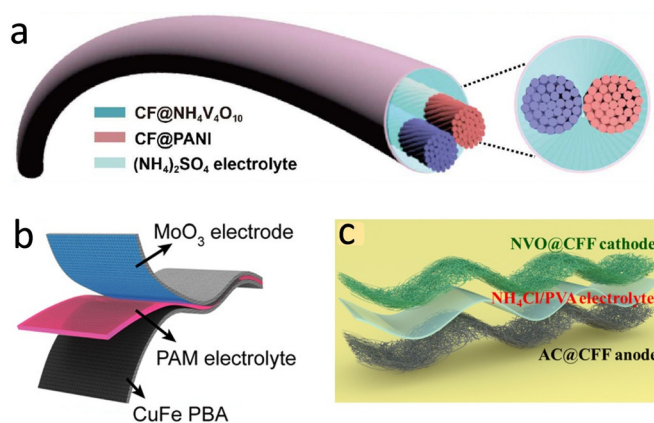


**Figure 8.** a) Schematic illustration of a flexible AAIB full cell consisting of a  $\text{CF@NH}_4\text{V}_4\text{O}_{10}$  cathode,  $\text{CF@PANI}$  anode, and 1M  $(\text{NH}_4)_2\text{SO}_4$  aqueous electrolyte. Reproduced from Ref. [34] with permission from Elsevier. b) Schematic illustration of a flexible full AAIB using an  $\text{h-MoO}_3$  anode,  $\text{CuFe}$  PBA cathode, and PAM hydrogel electrolyte. Reproduced from Ref. [60] with permission from John Wiley and Sons. c) Schematic illustration of the flexible quasi-solid-state device consisting of ammonium vanadium oxide on a carbon fiber felt ( $\text{NVO@CFF}$ ) cathode, active carbon on a carbon fiber felt ( $\text{AC@CFF}$ ) anode, and an  $\text{NH}_4\text{Cl/PVA}$  hydrogel electrolyte. Reproduced from Ref. [87] with permission from Elsevier.

offer excellent rate capability and durability,<sup>[24]</sup> as well as inherent safety and low-cost.<sup>[29]</sup> However, several challenges remain, such as limited options of electrode materials and limited energy density. To promote the development of AAIBs, the current existing problems with electrodes, electrolytes, and full cells are assessed in this section.

#### 5.1. Cathodes

PBAs are the most common cathode material for AAIBs (Table 1).<sup>[23]</sup> Although several types of PBAs have exhibited good performance, their specific capacity still seems unsatisfactory. Therefore, PBAs with high specific capacity, such as manganese hexacyanoferrate, could be further developed. Besides PBAs,<sup>[33]</sup> V-based<sup>[32]</sup> and Mn-based oxides<sup>[29]</sup> have also attracted attention because of their reversible capacity. However, their output potential is lower compared to PBAs, but some polyanionic compounds containing V–O or Mn–O bonds could be viable alternatives. Notably, these cathode materials demonstrated good durability after thousands of cycles at a high current density. However, the cycling stability at low current densities is often still unsatisfactory. More emphasis should be put on understanding the ageing phenomena leading to capacity fading and low coulombic efficiency. Comprehensive “post-mortem” analysis of electrodes (SEM, XRD, XPS) and electrolytes (ICP) may help to identify phase transitions, active material leaching, as well as precipitation of side products at the electrode/electrolyte interface. Parasitic reactions involving the electrolyte could also be probed by differential electrochemical mass spectrometry (DEMS).

### 5.2. Anodes

Organic compounds have demonstrated a favorable performance when employed as the anode materials of AAIBs (Table 2). However, like the cathode materials, the performance at low current rate and the possible accompanying fading mechanisms still requires extensive improvement. Additionally, the specific capacity of anode materials is typically low, thus organic materials possessing multiple functional groups (e.g. carbonyl groups) that could accommodate ammonium ions at a low potential are promising candidates for further development. Nevertheless, organic materials also suffer from low electrical conductivity and, therefore, the addition of a large amount of conductive additive is necessary. This can result in a low active material ratio and an electrode loading leading to poor gravimetric and volumetric energy density. To improve the conductivity, some organic composites with conductive carbon materials, for example, Ketjen Black,<sup>[61]</sup> were developed, but the ratio of the conductive carbon materials was as high as 50 wt%. Consequently, it is imperative to synthesize organic compounds that are uniformly distributed on the conductive matrix to minimize the amount of the conductive additive. Apart from organic compounds, metal oxides, such as h-MoO<sub>3</sub>, have delivered remarkable performance for the storage of NH<sub>4</sub><sup>+</sup> ions while its output potential is relatively high as an anode material.<sup>[60]</sup> Therefore, other types of metal oxides that could host NH<sub>4</sub><sup>+</sup> ions and possess a low output potential should be considered, such as Ti- or Fe-based oxides.

### 5.3. Electrolytes

Both conventional liquid and hydrogel electrolytes have been developed in the past few years (Figure 1b). In aqueous liquid electrolytes, (NH<sub>4</sub>)<sub>2</sub>SO<sub>4</sub>,<sup>[24]</sup> NH<sub>4</sub>Cl,<sup>[60]</sup> NH<sub>4</sub>Ac,<sup>[29]</sup> NH<sub>4</sub>NO<sub>3</sub><sup>[36]</sup> are employed as the single salt for the preparation of electrolytes. In addition to the conventional dilute electrolytes, highly concentrated NH<sub>4</sub>Ac with a widened ESW has been proposed and has led to an improved performance.<sup>[53]</sup> Moreover, limited amounts of additives were included to stabilize the electrode materials through the “common ion effect”.<sup>[38]</sup> From conventional aqueous liquid electrolytes, hydrogel electrolytes can also be obtained by adding poly-

mers, for example, PAM<sup>[60]</sup> and PVA,<sup>[87]</sup> which may accelerate the development of flexible NH<sub>4</sub><sup>+</sup> storage devices. Despite such promising results, many aspects regarding the nature of the interphases generated by such electrolytes remain elusive. Further studies are encouraged to understand the composition and properties of solid–electrolyte interphases by using, for example, XPS, soft X-ray absorption spectroscopy, transmission electron microscopy, and electrochemical impedance spectroscopy. In addition, the solvated structure of these electrolytes requires further investigation to elucidate the role of the unique tetrahedral structure of NH<sub>4</sub><sup>+</sup> ions. In this context, the combination of theoretical methods (e.g. molecular dynamics simulations) and experimental techniques (e.g. Raman, small- and wide-angle X-ray scattering, small-angle neutron scattering, etc.) could provide interesting insights.

### 5.4. Full Cells

Figure 9a shows a selection of representative full rocking-chair AAIBs. PBAs and organic materials are the most commonly adopted as the positive and negative electrode materials, respectively. The best performing combinations can deliver an average output voltage of around 1 V and specific capacity above 50 mAhg<sup>-1</sup> based on the active mass of both electrodes (Figure 9a), which certainly needs improvement. As displayed in Figure 9b, some systems, such as h-MoO<sub>3</sub>//CuFePBA and ALO//Ni-APW have considerable capacity retention even after thousands of cycles and a very high CE. Overall, although the cyclability and power density may be adequate, the energy density (Figure 9c) is still inferior compared with other aqueous batteries that use metallic charge carriers. A major hurdle is also represented by the fact that most cathode materials do not contain NH<sub>4</sub><sup>+</sup> ions in their native structure. A prospective solution would be to electrochemically ammoniate the cathode material in sacrificial cells before assembly in a full cell. As demonstrated by the Shu group, employing NH<sub>4</sub><sup>+</sup>-rich cathodes may be a strategy to counterbalance NH<sub>4</sub><sup>+</sup> consumption during long-term cycling.<sup>[35]</sup> Alternatively, cathode materials containing ammonium ions could be prepared by ion exchange. Conventional solid-state methods employed for electrode materials based on metallic charge carriers cannot be used because of the tendency of ammonium salts to thermally decompose. With

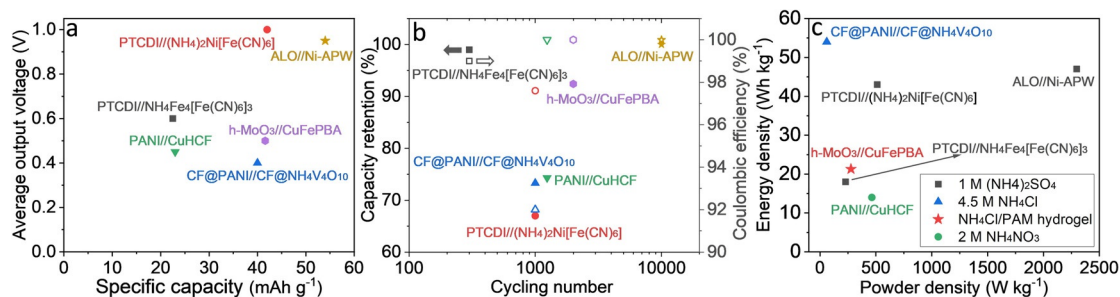


**Figure 9.** Performance of selected full rocking-chair AAIBs reported in the literature. a) Average output voltage as a function of the specific capacity. b) Capacity retention and CE as a function of the cycling number. c) Energy density as a function of power density. The specific capacity, energy density, and power density are calculated based on the total mass of both the cathode and anode active materials.

regards to anode materials, increasing the CE upon the first  $\text{NH}_4^+$  insertion is also important, especially when coupled with  $\text{NH}_4^+$ -deficient cathodes. In this respect, a proper balancing of the N/P (negative to positive) capacity ratio will also be fundamental to maximize cell performance.

### Acknowledgements

J.H. gratefully acknowledges financial support from the Chinese Scholarship Council. Financial support from the Helmholtz Association is also acknowledged. Open Access funding enabled and organized by Projekt DEAL.

### Conflict of Interest

The authors declare no conflict of interest.

**Keywords:** ammonium ions · aqueous electrolytes · batteries · electrode materials · storage mechanism

- [1] Z. Yang, J. Zhang, M. C. Kintner-Meyer, X. Lu, D. Choi, J. P. Lemmon, J. Liu, *Chem. Rev.* **2011**, *111*, 3577–3613.
- [2] D. Larcher, J.-M. Tarascon, *Nat. Chem.* **2015**, *7*, 19–29.
- [3] M. Y. Suberu, M. W. Mustafa, N. Bashir, *Renewable Sustainable Energy Rev.* **2014**, *35*, 499–514.
- [4] O. Schmidt, A. Hawkes, A. Gambhir, I. Staffell, *Nat. Energy* **2017**, *2*, 17110.
- [5] E. Goikolea, V. Palomares, S. Wang, I. R. de Larramendi, X. Guo, G. Wang, T. Rojo, *Adv. Energy Mater.* **2020**, *10*, 2002055.
- [6] D. Chao, W. Zhou, F. Xie, C. Ye, H. Li, M. Jaroniec, S.-Z. Qiao, *Sci. Adv.* **2020**, *6*, eaba4098.
- [7] W. Li, J. R. Dahn, D. S. Wainwright, *Science* **1994**, *264*, 1115–1118.
- [8] J. Huang, Z. Guo, Y. Ma, D. Bin, Y. Wang, Y. Xia, *Small Methods* **2019**, *3*, 1800272.
- [9] C. D. Wessells, S. V. Peddada, R. A. Huggins, Y. Cui, *Nano Lett.* **2011**, *11*, 5421–5425.
- [10] Y. Wang, L. Mu, J. Liu, Z. Yang, X. Yu, L. Gu, Y. S. Hu, H. Li, X. Q. Yang, L. Chen, *Adv. Energy Mater.* **2015**, *5*, 1501005.
- [11] Z. Li, D. Young, K. Xiang, W. C. Carter, Y.-M. Chiang, *Adv. Energy Mater.* **2013**, *3*, 290–294.
- [12] J. Han, A. Mariani, H. Zhang, M. Zarrabeitia, X. Gao, D. V. Carvalho, A. Varzi, S. Passerini, *Energy Storage Mater.* **2020**, *30*, 196–205.
- [13] D. Su, A. McDonagh, S. Z. Qiao, G. Wang, *Adv. Mater.* **2017**, *29*, 1604007.
- [14] N. Zhang, F. Cheng, J. Liu, L. Wang, X. Long, X. Liu, F. Li, J. Chen, *Nat. Commun.* **2017**, *8*, 405.
- [15] H. Pan, Y. Shao, P. Yan, Y. Cheng, K. S. Han, Z. Nie, C. Wang, J. Yang, X. Li, P. Bhattacharya, K. T. Mueller, J. Liu, *Nat. Energy* **2016**, *1*, 16039.
- [16] B. Tang, L. Shan, S. Liang, J. Zhou, *Energy Environ. Sci.* **2019**, *12*, 3288–3304.
- [17] J. Han, A. Mariani, A. Varzi, S. Passerini, *J. Power Sources* **2021**, *485*, 229329.
- [18] X. Sun, V. Duffort, B. L. Mehdi, N. D. Browning, L. F. Nazar, *Chem. Mater.* **2016**, *28*, 534–542.
- [19] F. Wang, X. Fan, T. Gao, W. Sun, Z. Ma, C. Yang, F. Han, K. Xu, C. Wang, *ACS Cent. Sci.* **2017**, *3*, 1121–1128.
- [20] R. Y. Wang, C. D. Wessells, R. A. Huggins, Y. Cui, *Nano Lett.* **2013**, *13*, 5748–5752.
- [21] C. Wu, S. Gu, Q. Zhang, Y. Bai, M. Li, Y. Yuan, H. Wang, X. Liu, Y. Yuan, N. Zhu, *Nat. Commun.* **2019**, *10*, 73.
- [22] Y. Gao, H. Yang, X. Wang, Y. Bai, N. Zhu, S. Guo, L. Suo, H. Li, H. Xu, C. Wu, *ChemSusChem* **2020**, *13*, 732–740.
- [23] C. D. Wessells, S. V. Peddada, M. T. McDowell, R. A. Huggins, Y. Cui, *J. Electrochem. Soc.* **2012**, *159*, A98.
- [24] X. Wu, Y. Qi, J. J. Hong, Z. Li, A. S. Hernandez, X. Ji, *Angew. Chem. Int. Ed.* **2017**, *56*, 13026–13030; *Angew. Chem.* **2017**, *129*, 13206–13210.
- [25] G. Liang, F. Mo, X. Ji, C. Zhi, *Nat. Rev. Mater.* **2021**, *6*, 109–123.
- [26] M. Saito, S. Kawaharasaki, K. Ito, S. Yamada, K. Hayamizu, S. Seki, *RSC Adv.* **2017**, *7*, 14528–14535.
- [27] K. Xu, *Chem. Rev.* **2004**, *104*, 4303–4418.
- [28] G. Pálincas, T. Radnai, G. I. Szász, K. Heinzinger, *J. Chem. Phys.* **1981**, *74*, 3522–3526.
- [29] Y. Song, Q. Pan, H. Lv, D. Yang, Z. Qin, M. Y. Zhang, X. Sun, X. X. Liu, *Angew. Chem. Int. Ed.* **2021**, *60*, 5718–5722; *Angew. Chem.* **2021**, *133*, 5782–5786.
- [30] Y. You, A. Manthiram, *Adv. Energy Mater.* **2018**, *8*, 1701785.
- [31] X. Wu, Y. Xu, H. Jiang, Z. Wei, J. J. Hong, A. S. Hernandez, F. Du, X. Ji, *ACS Appl. Energy Mater.* **2018**, *1*, 3077–3083.
- [32] S. Dong, W. Shin, H. Jiang, X. Wu, Z. Li, J. Holoubek, W. F. Stickle, B. Key, C. Liu, J. Lu, P. A. Greaney, X. Zhang, X. Ji, *Chem* **2019**, *5*, 1537–1551.
- [33] C. Li, D. Zhang, F. Ma, T. Ma, J. Wang, Y. Chen, Y. Zhu, L. Fu, Y. Wu, W. Huang, *ChemSusChem* **2019**, *12*, 3732–3736.
- [34] H. Li, J. Yang, J. Cheng, T. He, B. Wang, *Nano Energy* **2020**, *68*, 104369.
- [35] X. Zhang, M. Xia, T. Liu, N. Peng, H. Yu, R. Zheng, L. Zhang, M. Shui, J. Shu, *Chem. Eng. J.* **2020**, 127767.
- [36] X. Zhang, M. Xia, H. Yu, J. Zhang, Z. Yang, L. Zhang, J. Shu, *Nano-micro Lett.* **2021**, *13*, 139.
- [37] M. Xia, X. Zhang, H. Yu, Z. Yang, S. Chen, L. Zhang, M. Shui, Y. Xie, J. Shu, *Chem. Eng. J.* **2021**, *421*, 127759.
- [38] S. Li, M. Xia, C. Xiao, X. Zhang, H. Yu, L. Zhang, J. Shu, *Dalton Trans.* **2021**, *50*, 6520–6527.
- [39] J. Xing, X. Fu, S. Guan, Y. Zhang, M. Lei, Z. Peng, *Appl. Surf. Sci.* **2021**, *543*, 148843.
- [40] W. Xu, L. Zhang, K. Zhao, X. Sun, Q. Wu, *Electrochim. Acta* **2020**, *360*, 137008.
- [41] M. B. Robin, P. Day, in *Advances in inorganic chemistry and radiochemistry, Vol. 10*, Elsevier, Amsterdam, **1968**, pp. 247–422.
- [42] F. Herren, P. Fischer, A. Ludi, W. Hälg, *Inorg. Chem.* **1980**, *19*, 956–959.
- [43] H. Buser, D. Schwarzenbach, W. Petter, A. Ludi, *Inorg. Chem.* **1977**, *16*, 2704–2710.
- [44] K. Itaya, I. Uchida, V. D. Neff, *Acc. Chem. Res.* **1986**, *19*, 162–168.
- [45] K. Hurlbutt, S. Wheeler, I. Capone, M. Pasta, *Joule* **2018**, *2*, 1950–1960.
- [46] L. Fan, C. Jia, Y. G. Zhu, Q. Wang, *ACS Energy Lett.* **2017**, *2*, 615–621.
- [47] S. Qiu, Y. Xu, X. Wu, X. Ji, *Electrochem. Energy Rev.* **2021**, doi:10.1007/s41918-020-00088-x.
- [48] C. Erinwingbovo, M. S. Palagonia, D. Brogioli, F. La Mantia, *ChemPhysChem* **2017**, *18*, 917–925.
- [49] J. Bácskai, K. Martinusz, E. Czirik, G. Inzelt, P. Kulesza, M. Malik, *J. Electroanal. Chem.* **1995**, *385*, 241–248.
- [50] J. J. García-Jareño, D. Giménez-Romero, F. Vicente, C. Gabrielli, M. Keddad, H. Perrot, *J. Phys. Chem. B* **2003**, *107*, 11321–11330.
- [51] J. Agrisuelas, J. J. García-Jareño, F. Vicente, *J. Phys. Chem. C* **2012**, *116*, 1935–1947.
- [52] X. Zhang, M. Xia, T. Liu, N. Peng, H. Yu, R. Zheng, L. Zhang, M. Shui, J. Shu, *Chem. Eng. J.* **2021**, *421*, 127767.

- [53] S. Qiu, Y. Xu, X. Li, S. K. Sandstrom, X. Wu, X. Ji, *Electrochem. Commun.* **2021**, *122*, 106880.
- [54] D. Yang, Y. Song, M. Y. Zhang, Z. Qin, R. Dong, C. Li, X. X. Liu, *Adv. Funct. Mater.* **2021**, *31*, 2100477.
- [55] Y. Gao, H. Yang, Y. Bai, C. Wu, *J. Mater. Chem. A* **2021**, *9*, 11472–11500.
- [56] L. Cao, D. Li, T. Deng, Q. Li, C. Wang, *Angew. Chem. Int. Ed.* **2020**, *59*, 19292–19296; *Angew. Chem.* **2020**, *132*, 19454–19458.
- [57] D. Wang, L. Wang, G. Liang, H. Li, Z. Liu, Z. Tang, J. Liang, C. Zhi, *ACS Nano* **2019**, *13*, 10643–10652.
- [58] J. Han, H. Euchner, M. Kuenzel, S. M. Hosseini, A. Groß, A. Varzi, S. Passerini, *ACS Energy Lett.* **2021**, *6*, 3063–3071.
- [59] J. J. Holoubek, H. Jiang, D. Leonard, Y. Qi, G. C. Bustamante, X. Ji, *Chem. Commun. (Camb)* **2018**, *54*, 9805–9808.
- [60] G. Liang, Y. Wang, Z. Huang, F. Mo, X. Li, Q. Yang, D. Wang, H. Li, S. Chen, C. Zhi, *Adv. Mater.* **2020**, *32*, 1907802.
- [61] G. Zhou, X. An, C. Zhou, Y. Wu, Y.-E. Miao, T. Liu, *Compos. Commun.* **2020**, *22*, 100519.
- [62] Y. Ma, T. Sun, Q. Nian, S. Zheng, T. Ma, Q. Wang, H. Du, Z. Tao, *Nano Res.* **2021**, <https://doi.org/10.1007/s12274-021-3777-1>.
- [63] M. Naguib, V. N. Mochalin, M. W. Barsoum, Y. Gogotsi, *Adv. Mater.* **2014**, *26*, 992–1005.
- [64] M. Naguib, O. Mashtalir, J. Carle, V. Presser, J. Lu, L. Hultman, Y. Gogotsi, M. W. Barsoum, *ACS Nano* **2012**, *6*, 1322–1331.
- [65] O. Mashtalir, M. Naguib, V. N. Mochalin, Y. Dall'Agnese, M. Heon, M. W. Barsoum, Y. Gogotsi, *Nat. Commun.* **2013**, *4*, 1716.
- [66] J. Come, M. Naguib, P. Rozier, M. W. Barsoum, Y. Gogotsi, P.-L. Taberna, M. Morcrette, P. Simon, *J. Electrochem. Soc.* **2012**, *159*, A1368.
- [67] M. R. Lukatskaya, O. Mashtalir, C. E. Ren, Y. Dall'Agnese, P. Rozier, P. L. Taberna, M. Naguib, P. Simon, M. W. Barsoum, Y. Gogotsi, *Science* **2013**, *341*, 1502–1505.
- [68] J.-Y. Luo, Y.-Y. Xia, *J. Power Sources* **2009**, *186*, 224–227.
- [69] L. Chen, J. Liu, Z. Guo, Y. Wang, C. Wang, Y. Xia, *J. Electrochem. Soc.* **2016**, *163*, A904.
- [70] J. Han, M. Zarrabeitia, A. Mariani, Z. Jusys, M. Hekmatfar, H. Zhang, D. Geiger, U. Kaiser, R. J. Behm, A. Varzi, S. Passerini, *Nano Energy* **2020**, *77*, 105176.
- [71] H.-S. Kim, J. B. Cook, H. Lin, J. S. Ko, S. H. Tolbert, V. Ozolins, B. Dunn, *Nat. Mater.* **2017**, *16*, 454–460.
- [72] L. Zheng, Y. Xu, D. Jin, Y. Xie, *Chem. Mater.* **2009**, *21*, 5681–5690.
- [73] Y. Zhang, Y. An, B. Yin, J. Jiang, S. Dong, H. Dou, X. Zhang, *J. Mater. Chem. A* **2019**, *7*, 11314–11320.
- [74] Y. Liang, Z. Tao, J. Chen, *Adv. Energy Mater.* **2012**, *2*, 742–769.
- [75] Y. Liang, Y. Yao, *Joule* **2018**, *2*, 1690–1706.
- [76] Y. Xu, M. Zhou, Y. Lei, *Mater. Today* **2018**, *21*, 60–78.
- [77] Z. Song, H. Zhou, *Energy Environ. Sci.* **2013**, *6*, 2280–2301.
- [78] Y. Lu, J. Chen, *Nat. Rev. Chem.* **2020**, *4*, 127–142.
- [79] W. Deng, Y. Shen, J. Qian, Y. Cao, H. Yang, *ACS Appl. Mater. Interfaces* **2015**, *7*, 21095–21099.
- [80] Z. Song, H. Zhan, Y. Zhou, *Angew. Chem. Int. Ed.* **2010**, *49*, 8444–8448; *Angew. Chem.* **2010**, *122*, 8622–8626.
- [81] L. Suo, O. Borodin, T. Gao, M. Olguin, J. Ho, X. Fan, C. Luo, C. Wang, K. Xu, *Science* **2015**, *350*, 938–943.
- [82] W. Sun, F. Wang, S. Hou, C. Yang, X. Fan, Z. Ma, T. Gao, F. Han, R. Hu, M. Zhu, *J. Am. Chem. Soc.* **2017**, *139*, 9775–9778.
- [83] G. Liang, F. Mo, H. Li, Z. Tang, Z. Liu, D. Wang, Q. Yang, L. Ma, C. Zhi, *Adv. Energy Mater.* **2019**, *9*, 1901838.
- [84] X. Wu, J. J. Hong, W. Shin, L. Ma, T. Liu, X. Bi, Y. Yuan, Y. Qi, T. W. Surta, W. Huang, J. Neufeind, T. Wu, P. A. Greaney, J. Lu, X. Ji, *Nat. Energy* **2019**, *4*, 123–130.
- [85] Y. Liao, H. C. Chen, C. Yang, R. Liu, Z. Peng, H. Cao, K. Wang, *Energy Storage Mater.* **2022**, *44*, 508–516.
- [86] W. Liu, X. Zhang, Y. Huang, B. Jiang, Z. Chang, C. Xu, F. Kang, *J. Energy Chem.* **2021**, *56*, 365–373.
- [87] P. Wang, Y. Zhang, H. Jiang, X. Dong, C. Meng, *Chem. Eng. J.* **2022**, *427*, 131548.
- [88] S. Huang, F. Wan, S. Bi, J. Zhu, Z. Niu, J. Chen, *Angew. Chem. Int. Ed.* **2019**, *58*, 4313–4317; *Angew. Chem.* **2019**, *131*, 4357–4361.
- [89] C. Yang, J. Chen, T. Qing, X. Fan, W. Sun, A. von Cresce, M. S. Ding, O. Borodin, J. Vatamanu, M. A. Schroeder, N. Eidson, C. Wang, K. Xu, *Joule* **2017**, *1*, 122–132.
- [90] H. J. Kwon, Y. Osada, J. P. Gong, *Polym. J.* **2006**, *38*, 1211–1219.
- [91] Z. Wang, H. Li, Z. Tang, Z. Liu, Z. Ruan, L. Ma, Q. Yang, D. Wang, C. Zhi, *Adv. Funct. Mater.* **2018**, *28*, 1804560.

Manuscript received: November 5, 2021

Accepted manuscript online: December 15, 2021

Version of record online: February 23, 2022